Green Chemistry

PAPER

View Article Online
View Journal | View Issue

Cite this: *Green Chem.*, 2025, **27**, 2578

Efficient and switchable production of bio-diol/triol chemicals from 5-hydroxymethylfurfural†

Armin Rezayan, [a,b] Dan Wu, [b] Zhen Zhang,[b] Xiaomeng Yang,[b] Renfeng Nie,[b] Tianliang Lu, [b] Jianshe Wang, [b] Xiaoqin Si,[b] Yongsheng Zhang*[b] and Chunbao Xu *[a]

5-Hydroxymethylfurfural (HMF), regarded as one of the top bio-based platform chemicals, possesses a molecular structure with C=O, C–OH, and a furan ring, allowing for its conversion into a variety of high value-added green chemicals through a range of catalytic reactions. This study focuses on the highly promising yet challenging conversion of HMF into furanic and non-furanic chemicals with tunable selectivity *via* hydrogenation/hydrogenolysis over cobalt–copper–aluminum layered double oxide (Co_xCuAl LDO) catalysts. The synthesized Co_xCuAl catalysts were meticulously characterized and then utilized for the efficient transformation of HMF into 2,5-bis(hydroxymethyl)furan (BHMF) and 1,2,6-hexanetriol (1,2,6-HTO). The CoAl, CuAl, and physically mixed CoAl + CuAl catalysts predominantly favored BHMF production *via* hydrogenation of HMF's carbonyl group. However, the optimal Co_5CuAl catalyst achieved efficient and switchable production of BHMF (~91% yield) or 1,2,6-HTO (~72% yield) under tunable reaction conditions, owing to the synergistic effects of CoCu in modifying electronic–geometric properties, where the electron-enriched Co facilitated ring-opening hydrogenolysis. Indeed, the formed CoCu interface/alloy is capable of both hydrogenation and ring-opening hydrogenolysis, enabling adjustable product formation; however, the absence of this active site in monometallic catalysts hinders ring-opening hydrogenolysis, resulting in the production of a non-switchable product, BHMF. Density functional theory (DFT) calculations and experimental studies disclosed that the bimetallic catalyst outperformed its monometallic counterpart in terms of HMF and H adsorption, which can be attributed to the formation of the CoCu alloy, inducing a modified d-band center. The findings and future development of this work would lead to sustainable production of high value-added bio-diols/triols from bioresources.

Received 18th November 2024,
Accepted 29th January 2025

DOI: 10.1039/d4gc05875e

rsc.li/greenchem

Green foundation

1. This study showcases an efficient catalytic system for producing high-value bio-based diol/triol chemicals (BHMF and 1,2,6-HTO) from biomass-derived HMF. These chemicals have potential applications across various fields, enabling the synthesis of green chemicals and materials such as resins, fibers, polymers, polyurethanes, and drugs. Thus, this work represents a significant step towards the production of green and sustainable materials with low carbon emissions, contributing to the field of green chemistry.
2. This study illustrates the switchable production of BHMF and 1,2,6-HTO from HMF through hydrogenation/ring-opening hydrogenolysis with high yields of 91% and 72%, respectively, achieved using a bimetallic Co_5CuAl catalyst, attributed to its modified electro-geometric properties compared to monometallic CoAl and CuAl catalysts.
3. This work can be made even more environmentally friendly in two ways. One approach involves preparing the CoCu catalyst using solvent-free techniques, which could substantially reduce the waste generated during the catalyst synthesis process. Another approach includes separating and reusing the catalytic reaction solvent, which is highly appealing from a green sustainability perspective.

Introduction

Biomass is considered a sustainable and carbon-neutral alternative to fossil resources for the production of fuels, chemicals and materials.[1] 5-Hydroxymethylfurfural (HMF) has

[a]*School of Energy and Environment, City University of Hong Kong, Kowloon, Hong Kong SAR. E-mail: chunbaxu@cityu.edu.hk*
[b]*School of Chemical Engineering, Zhengzhou University, Zhengzhou 450001, China. E-mail: yzhang@zzu.edu.cn*
† Electronic supplementary information (ESI) available. See DOI: https://doi.org/10.1039/d4gc05875e

been regarded as one of the top bio-based platform chemicals derived from biomass (sugars, starch, cellulose or lignocellulose). It possesses a molecular structure with C=O, C–OH, and a furan ring, allowing for its conversion into a variety of green chemicals through a range of reactions including oxidation, hydrogenation, hydrogenolysis, rehydration, etherification, *etc.*[2] Among these chemicals, two high value-added derivatives from HMF are 2,5-bis(hydroxymethyl)furan (BHMF) and 1,2,6-hexanetriol (1,2,6-HTO), which can be obtained through hydrogenation and/or hydrogenolysis reactions. BHMF finds applications in the synthesis of resins, fibers, polymers, polyurethanes, and drugs,[3] while 1,2,6-HTO is used as a humectant, solvent, and plasticizer in cosmetics, pharmaceuticals, and personal care products, as well as a precursor for polyurethanes and polyester resins.[4]

Achieving selective conversion of HMF to BHMF involves the hydrogenation of the carbonyl group to alcohol while avoiding the hydrogenation of the furan ring,[5] and the conversion of HMF to 1,2,6-HTO is achieved through hydrogenation and ring-opening hydrogenolysis reactions.[6] However, these catalytic systems also yield various other byproducts such as 5-methylfurfural (5-MF), 2,5-dimethylfuran (DMF), 2,5-dimethyltetrahydrofuran (DMTHF), 1,5-hexanediol (1,5-HDO), *etc.*, resulting in reduced selectivity for the desired target products (Scheme 1).[7] Therefore, achieving highly selective transformation of HMF into furanic diols and non-furanic triols is an appealing yet extremely challenging objective.

Considerable efforts have been dedicated to developing supported metal catalysts (such as Pt, Au, and Ru) for the selective conversion of HMF to the aforementioned chemicals (BHMF and 1,2,6-HTO). For instance, Wang *et al.*[8] achieved ~82% yield of BHMF using a Ru/Co_3O_4 catalyst at 190 °C for 6 h with isopropanol as a hydrogen donor. In another study, Kataoka *et al.*[9] promoted Pt/CeO_2 with Co and achieved up to 42% yield of 1,2,6-HTO at 135 °C and 3 MPa for 24 h. However, the use of expensive noble metal catalysts remains a challenge for large-scale applications, leading to increasing attention towards non-noble metal catalysts like Ni, Cu, and Co, known for their hydrogenation and hydrogenolysis capabilities.[10] Wang *et al.*[11] prepared a $Cu/MgAlO_x$ catalyst and obtained an optimal yield of ~92% of BHMF at 180 °C for 5 h. In a study by Yao *et al.*,[12] a mixed Ni and Co oxide catalyst demonstrated acceptable activity for 1,2,6-HTO production, with up to 63% yield after 12 h of reaction. Nevertheless, these systems encountered challenges such as high temperature/pressure requirements and a long reaction time. Additionally, very few studies have introduced a single catalyst that efficiently produces both BHMF and 1,2,6-HTO. Consequently, there is significant interest in exploring stable, eco-friendly, and efficient non-noble catalysts that can produce versatile products (in this case BHMF and 1,2,6-HTO) from HMF under mild reaction conditions.

Cobalt–copper mixed oxide catalysts have a synergistic effect between the Co and Cu metals (electronic–geometric effects), demonstrating enhanced catalytic activity and product selectivity in various reactions, including hydrogenation and hydrogenolysis. Cai *et al.*[13] achieved a remarkable 78.4% glycerol conversion with ~84% selectivity towards 1,2-propanediol using a Cu–Co–Al catalyst, surpassing the performance of monometallic Co–Al and Cu–Al catalysts. In another study, a Co–Cu supported catalyst prepared *via* the impregnation method exhibited an excellent selectivity of 78% towards 2-methylfuran in furfural hydrogenation at 220 °C and 4 MPa.[14] Given the demonstrated hydrogenation and hydrogenolysis capabilities of Co–Cu catalysts in various catalytic systems, this composite holds significant potential for selectively transforming HMF into diverse furanic and non-furanic diols/triols.

The utilization of layered double hydroxide (LDH) and its metal oxide derivative obtained after calcination (LDO) has been widespread in numerous catalytic reactions, resulting in improved metal dispersion, catalytic activity, and product selectivity.[15,16] Hence, in this work, for the first time, Co_xCuAl-LDO catalysts were introduced as promising catalysts for switchable production of BHMF and 1,2,6-HTO in high yields by hydrogenation/hydrogenolysis of HMF through a one-pot process under tunable conditions. Comprehensive analyses of the synthesized catalysts were conducted and theoretical calculations were performed to investigate the relationship between their structure and product selectivity in catalytic tests. Additionally, various experimental conditions such as catalyst reduction temperature, Co/Cu molar ratio, reaction tempera-

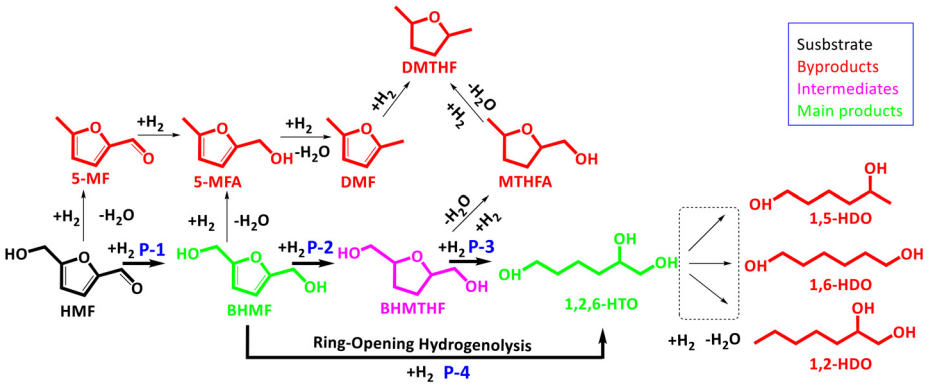

Scheme 1 The reaction pathways for HMF conversion into BHMF and 1,2,6-HTO.

ture/time, hydrogen pressure, *etc.* were examined to achieve the highest possible yield and selectivity of target products (BHMF and 1,2,6-HTO). Furthermore, the stability of the optimal catalyst was evaluated to assess its potential for large-scale application and the plausible reaction mechanisms over the catalyst were discussed through product/intermediate investigation, controlled experiments and absorption tests.

Experimental

Materials

A series of cobalt–copper–aluminum LDO catalysts were prepared using the following chemicals: aluminum nitrate nonahydrate (Rhawn, 99%), copper nitrate trihydrate (Rhawn, 99%), cobalt nitrate hexahydrate (Rhawn, 99.99%), sodium hydroxide (Yongda, 99%), and sodium carbonate anhydrous (Yongda, ≥99.8%). In addition, the following chemicals and solvents were used in the HMF hydrogenation/hydrogenolysis experiments: 5-hydroxymethylfurfural (HMF, Macklin, 97%), 2,5-bis (hydroxymethyl)tetrahydrofuran (BHMTHF, Macklin, 98%), 2,5-bis(hydroxymethyl)furan (BHMF, Macklin, ≥98%), 2,5-dimethylfuran (DMF, Macklin, 99%), 5-methylfurfural (5-MF, Rhawn, 99%), 5-methylfurfurylalcohol (5-MFA, Rhawn, 98%), 1,2,6-hexanetriol (1,2,6-HTO, Energy Chemical, 98%), 1,2-hexanediol (1,2-HDO, Macklin, 98%), 1,6-hexanediol (1,6-HDO, Rhawn, 99.5%), tridecane (Rhawn, 98%), methanol (Yongda, ≥99.5%), ethanol (Yongda, ≥99.7%), propanol (Yongda, 99.8%), butanol (Rhawn, 99%), and isopropanol (Yongda, ≥99.7%). All chemicals were used as received.

Preparation of catalysts

Various CoCuAl LDO catalysts at a constant (Co + Cu)/Al = 3 molar ratio were synthesized using the facile co-precipitation technique, modified from ref. 17. Briefly, calculated amounts of $Al(NO_3)_3{\cdot}9H_2O$, $Co(NO_3)_2{\cdot}6H_2O$, and $Cu(NO_3)_2{\cdot}3H_2O$ (with a total metal content of 4.2 mmol) were added into 30 mL of deionized water and agitated at room temperature for 0.5 h to achieve a uniform solution. Subsequently, a mixed alkaline solution of NaOH (2 M) + Na_2CO_3 (1 M) was added dropwise into the prepared solution to adjust the pH to ~10. The formed suspension was then placed in an oil bath and stirred under reflux for 24 h at 65 °C. The resulting precipitate was filtered, washed four times with water, and dried at 60 °C for 12 h. The obtained solids were calcined at 500 °C for 4 h in air and freshly reduced at 500 °C for 3 h using H_2 before conducting the reactions. The synthesized LDO catalysts were denoted as Co_xCuAl catalysts, where x represents the theoretical Co/Cu molar ratio. Additionally, monometallic CoAl and CuAl catalysts were also synthesized using the same procedure mentioned above, without adding copper and cobalt salts, respectively, while in the reactions with the CoAl catalyst, the catalyst was reduced at 700 °C according to its H_2-TPR pattern. According to ICP analysis, the wt% of Co, Cu, and Al are as follows: 67.3 wt% Co and 11.3 wt% Al in CoAl, 72.1 wt% Cu and 10.2 wt% Al in CuAl, and 12.2 wt% Cu, 52.7 wt% Co, and 9.7 wt% Al in Co_5CuAl.

Characterization of catalysts

X-ray diffraction (XRD) analysis was conducted using Cu K_α radiation in the scan range of 2θ = 10–80° (Bruker D8 Advance). A physisorption analyzer (Micrometrics ASAP-2460) was utilized to measure the catalysts' surface area and pore diameter/volume. Prior to the tests, the samples underwent a degassing process for 3 h at 150 °C. Transition electron microscopy (TEM) and high-resolution TEM (HR-TEM) analyses were conducted using a resolution of 1.4 Å and an acceleration voltage of 200 kV (JEM-2100F). X-ray photoelectron spectroscopy (XPS) analysis coupled with *in situ* catalyst reduction was conducted to determine the valence state of elements (AXIS Supra$^+$). For the peak analysis, the XPSPEAK41 software was used, with the binding energy values calibrated using the C 1s peak at 284.6 eV, and Shirley was considered as a background type. Thermal gravimetric analysis (TGA) was carried out under N_2 in the temperature range of 30–800 °C (STA 8000) to validate the presence of carbonaceous materials on the surface of the spent catalysts. CO-FTIR spectroscopy was performed using a Bruker Vertex-70 infrared spectrometer to study the behavior of the surface active sites of the mono-/bimetallic LDO catalysts. Hydrogen and ammonia temperature-programmed desorption (H_2/NH_3-TPD) and hydrogen temperature-programmed reduction (H_2-TPR) analyses were performed using a chemisorption device (Auto Chem II 2920) to determine the redox/acidic characteristics of the catalysts. The magnetization properties of the catalysts were measured using a vibrating sample magnetometer (VSM; LakeShore7404) at room temperature, over a magnetic field range of −20 000 to 20 000 Oe. ICP-AES analysis was carried out (Shimadzu ICPE-9820) to ascertain the weight percentages of cobalt and copper in the synthesized catalysts.

X-ray absorption spectroscopy (XAS) was conducted at the BL16U1 station in the Shanghai Synchrotron Radiation Facility (SSRF, 3.5 GeV, 250 mA), and the data were collected at room temperature. The samples were formed into 13 mm diameter discs with a thickness of 1 mm, utilizing graphite powder as a binding agent. The obtained XAFS data were processed in Athena to calibrate the background, pre-edge line, and post-edge line. Subsequently, Fourier transform fitting procedures were conducted using Artemis.[18]

An ultraviolet-visible spectrophotometer (UV-Vis; PerkinElmer Lambda 750) was employed to conduct the HMF adsorption experiments.[19] Initially, a specific quantity of HMF was dissolved in methanol to create the reference solution. Subsequently, 50 mg of catalyst (CoAl, CuAl, and Co_5CuAl) was added to 5 mL of the reference solution and mixed at room temperature for 2 h. Afterward, the resulting mixture was filtered, and the obtained solution was subjected to HMF adsorption tests.

Catalytic reactions and analysis of products

Catalytic hydrogenation/hydrogenolysis reactions of HMF were carried out in 30 mL parallel high-pressure reactors (Anhui Kemi Instrument Co., Ltd). In detail, an LDO catalyst (30 mg),

methanol (10 mL), HMF (1 mmol), and tridecane (40 mg as the internal standard for data analysis *via* GC) were loaded into the reactor and purged with H_2, followed by pressurization to the specified pressure. Then, the catalytic reaction was performed under pre-determined temperature/time conditions. After the completion of the reaction, the reactor was rapidly cooled in an ice-bath and then opened, and the mixture was filtered. The filtered product was collected for analysis. To ensure the reproducibility of the results, all experiments were repeated at least twice.

In this study, due to the close retention times of HMF and BHMF in GC analysis, which pose challenges in peak separation, their concentrations were analyzed using an Agilent 1220 Infinity II high-performance liquid chromatography (HPLC) system equipped with UV detectors at 232 nm and 284 nm, respectively. To detect HMF, a mobile phase comprising 80 v% water and 20 v% methanol was employed, while for BHMF measurement, the mobile phase comprised 95 v% water and 5 v% methanol. All HPLC analyses were carried out with a mobile phase flow rate of 1 mL min^{-1}. Concentrations of other products (BHMTHF, DMF, 5-MF, 5-MFA, 1,2,6-HTO, 1,2-HDO, and 1,6-HDO) were measured using a gas chromatography (GC, Fuli Instruments GC-9790Plus) system equipped with a flame ionization detector (FID) set at 280 °C and an HP-5 column. Peaks of the standard sample and some GC patterns of the obtained results are shown in Fig. S1.†

Based on the obtained calibration curves, the conversion of HMF and the yields of products are calculated using the following equations:

$$\text{Conversion}_{\text{HMF}}\ (\text{mol}\%) = 1 - \frac{\text{Residual moles of HMF}}{\text{Initial moles of HMF}} \times 100\% \quad (1)$$

$$\text{Yield}_{\text{Product}}\ (\text{mol}\%) = \frac{\text{Moles of the product}}{\text{Initial moles of HMF}} \times 100\% \quad (2)$$

Additionally, to quantitatively compare the results obtained in this work with those reported in the literature and to suppress possible errors due to the unavailability of the exact catalyst active sites (metal and/or acid sites), *specific productivity* (mmol g^{-1} h^{-1}) was calculated as an alternative to *turnover frequency* (TOF). In this case, the total weight of the catalyst was considered instead of the moles of catalyst active sites used in TOF calculations.

For the reusability tests, after each reaction run, the spent catalyst was separated using a magnet, washed with an acetone–methanol mixture, and reused in the subsequent reaction run. Catalyst regeneration involved vacuum drying and re-reduction under H_2 at 500 °C for 1 h.

Density functional theory calculations

First-principles methodologies[20] were employed for spin-polarization density functional theory (DFT) calculations, implementing the Perdew–Burke–Ernzerhof (PBE) formulation within the framework of generalized gradient approximation (GGA).[21] A plane wave basis set with a kinetic energy cutoff set at 450 eV was utilized alongside selected projected augmented wave (PAW) potentials to describe the ionic cores and to account for valence electrons.[22] Additionally, the van der Waals interactions were considered and incorporated using Grimme's DFT-D3 method.[23] The electronic energy achieved self-consistency when the change in energy fell below 10^{-5} eV, and the convergence criteria for geometry optimization were met when the energy change was below 0.02 eV $Å^{-1}$. Relaxation involved the use of a 2 × 2 × 1 gamma-centered grid in the Brillouin zone, with the addition of a 15 Å vacuum layer to the surface to prevent unwanted interactions among periodic images. The computations involved spin-polarized calculations. The adsorption energy $E_{(ads)}$ was calculated as follows: $E_{(ads)} = E_{(total)} - E_{(slab)} - E_{(adsorbate)}$, where $E_{(total)}$ represents the total energy of an optimized slab with the adsorbate, $E_{(slab)}$ represents the energy of a relaxed clean slab, and $E_{(adsorbate)}$ denotes the energy of an adsorbate molecule.

Results and discussion

Catalyst characterization

As illustrated in Fig. S2a,† the XRD patterns of the monometallic CoAl and CuAl catalysts before reduction contain apparent peaks corresponding to the Co_3O_4 (PDF#78-1969) and CuO (PDF#48-1548) phases.[24,25] In the Co_xCuAl samples, with increasing cobalt amount (decreasing copper concentration), the intensity of the CuO peaks dramatically declined, while the Co_3O_4 peaks gradually emerged due to the replacement of Cu^{2+} with Co^{2+} in the catalysts and the formation of smaller and/or homogeneously distributed CuO by insertion of Co into the samples' crystalline structure.[26] Furthermore, owing to the amorphous nature of Al oxide, no Al-related peaks were detected.[27] After reduction (Fig. S2b†), two weak peaks attributed to Cu_2O (PDF#99-0041) and three intense peaks assigned to the metallic Cu (PDF#85-1326) are observed in the CuAl catalyst, as well as XRD lines of CoO (PDF#72-1474) and metallic Co (PDF#15-0806) in the CoAl catalyst.[28,29] In the reduced Co_xCuAl samples, however, when $1 \leq x \leq 10$, no obvious XRD peak could be detected, suggesting highly dispersed metals with fine crystal size after reduction (Table S1†).

According to the physisorption tests, all the reduced catalyst samples exhibit type IV isotherms with an H3 hysteresis loop, indicating their mesoporous characteristics (Fig. S3a†), aligning with the findings in the pore size distributions determined *via* the BJH method (Fig. S3b†). As listed in Table S1,† CuAl and CoAl possess the lowest (57 m^2 g^{-1}) and highest (151 m^2 g^{-1}) BET_{SSA}, respectively. Increasing the cobalt content in Co_xCuAl results in a continuous increase in both BET_{SSA} and pore volume, implying reduced catalyst crystallinity and/or improved metals' dispersion due to the insertion of Co and a subsequent reduction in metal particle size (in agreement with the particle sizes obtained using the Scherrer equation, Table S1†).[28] Considering the textural properties of the catalysts reported in Table S1,† it can also be inferred that the larger particle size of Cu blocks/occupies some of the pores

and external surfaces of the catalyst support (alumina), resulting in a decrease in the SSA and pore volumes compared to CoAl. Additionally, it may block most micropores and small mesopores and/or create some voids, leading to an increase in the average pore sizes compared to CoAl.

As seen in the TEM image (Fig. 1a) and the corresponding particle size distribution (inset of Fig. 1a), the particle size of the metals in the Co_5CuAl catalyst shows a uniform distribution, mostly in the range of 10–20 nm with an average size of 15.96 nm. According to the lattice measurements from the HR-TEM image (Fig. 1b), various lattice orientations with lattice spacings of 0.205 nm, 0.207 nm, 0.209 nm, and 0.240 nm attributed to Co (111), CoCu (111), Cu (111), and CoO (110), respectively, were detected.[27,30,31] The presence of CoO is likely a result of incomplete reduction of Co_3O_4 and/or mild surface oxidation of the catalyst upon exposure to air, owing to the high oxophilicity of Co. Furthermore, the selected area electron diffraction (SAED) pattern (Fig. 1c) also demonstrates the diffraction rings of the different phases of Cu, Co, and the CoCu alloy. In the high-angle annular dark-field scanning transmission electron microscopy (HAADF-STEM) image (Fig. 1d), a random line scan using STEM-EDX mode reveals the consistent, homogeneous presence of both Co and Cu, with Co exhibiting higher intensity due to its elevated concentration in the prepared catalyst. These results demonstrate a close interaction between Co and Cu, indicating the formation of an alloy between them. The mapping analysis also validated the well-dispersed arrangement of elements in Co_5CuAl, demonstrating that Co and Cu were uniformly distributed within the catalyst (Fig. 1e).

As shown in the H_2-TPR patterns (Fig. 2a), the monometallic CuAl catalyst exhibits one H_2 consumption peak at 235 °C, ascribed to the reduction of CuO to Cu^0.[32] Besides, CoAl demonstrates distinct peaks at 339 °C, assigned to the reduction of Co_3O_4 to CoO, and at 700 °C, attributed to the reduction of CoO to metallic Co.[17] In the bimetallic Co_xCuAl catalysts, the peaks corresponding to the reduction of Co_3O_4 to CoO and CoO to Co^0 exhibit a shift towards much lower temperatures, with the respective peaks centering at 170–220 °C and 350–370 °C,[27] implying the H spill-over effect from easily reducible copper to cobalt oxides and thus facilitating their reduction.[33,34] The extent of this shift was found to be influenced by the Co/Cu ratio. Additionally, increasing the Co/Cu ratio from 0.1 to 10.0 shifts the CuO reduction peak towards lower temperatures, resulting in the splitting of a single peak into two peaks. The lower temperature peak could be associated with the reduction of finely dispersed CuO, whereas the higher temperature peak could be attributed to the reduction of the bulk CuO and/or $CuAl_2O_4$ spinel phases.[24,35] These changes suggest that the inclusion of Co enhances both the dispersion and the reducibility of Cu, while also promoting the reducibility of Co itself.[36] The H_2-TPD patterns of the reduced mono/bimetallic LDOs are shown in Fig. 2b. CoAl and CuAl exhibit broad and low-intensity peaks spanning from 50 °C to 500 °C, attributed to the chemisorbed hydrogen on the metallic state.[27] In contrast, Co_5CuAl shows a higher peak intensity, indicating a greater availability of surface active-H resulting from the H spill-over effect and a strong Co and Cu synergistic effect (Co–Cu alloy formation), which improves H_2 adsorption/activation capacity due to the electron enrichment of cobalt and/or electron-deficient copper (as shown later), thus likely contributing to its excellent catalytic performances in hydrogenation/hydrogenolysis of HMF.

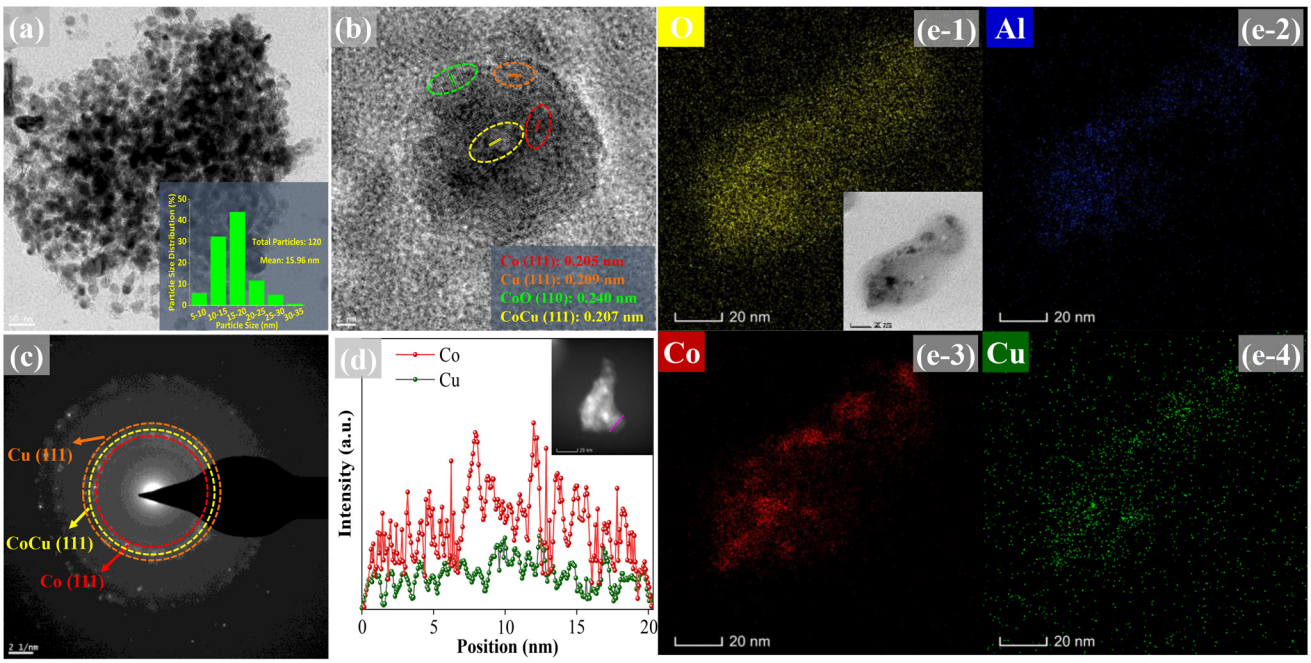

Fig. 1 TEM (a), HR-TEM (b), SAED (c), HAADF-STEM line scan (d), and mapping (e1–4) of the reduced Co_5CuAl catalyst.

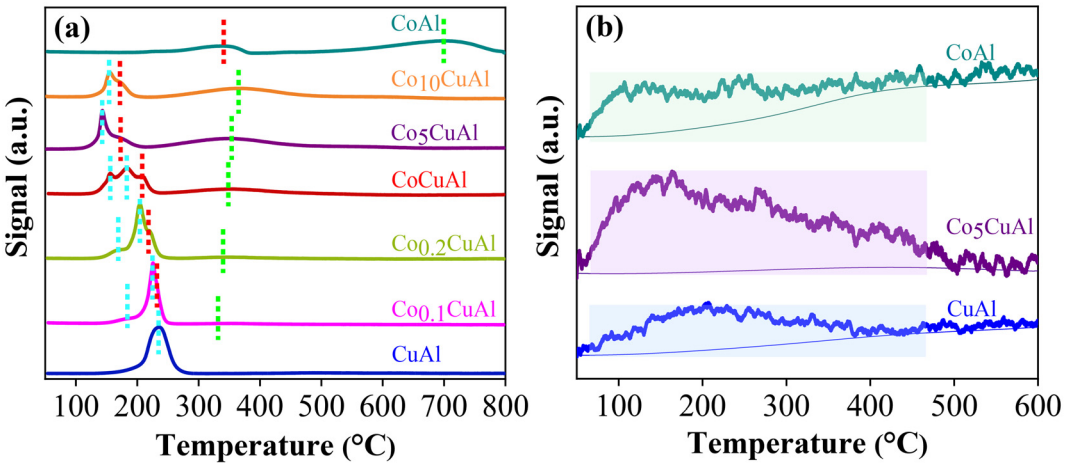

Fig. 2 (a) H_2-TPR and (b) H_2-TPD patterns of various LDOs.

XPS analysis coupled with *in situ* catalyst reduction was performed to investigate the surface compositions and chemical states of the reduced mono/bimetallic LDO catalysts. The Cu 2p spectra of CuAl and Co_5CuAl (Fig. 3a) exhibit well-defined peaks, corresponding to $Cu^{0/+}$ states (at 932.6 eV and 952.8 eV), and low-intensity, broad satellite peak regions.[37,38] The Co 2p spectra (Fig. 3b) can be deconvoluted into three distinct peaks representing Co^0 (major), Co^{2+} (minor), and satellite peaks.[36] Notably, a clear ~0.8–1.1 eV down-shift and up-shift in the Co 2p and Cu 2p patterns were observed, respectively, when comparing the monometallic CoAl or CuAl catalyst with the Co_5CuAl catalysts (Fig. 3a and b), suggesting electron transfer from Cu to Co in the bimetallic catalyst,[30] revealing the formation of the CoCu interface (alloy). The survey scan of the Co_5CuAl catalyst and the corresponding atomic percentages can be found in Fig. S4.†

To gain more detailed structural insights into the Co–Cu bimetallic catalyst, XAS was performed on Co_5CuAl. The X-ray absorption near edge spectroscopy (XANES) pattern of the Cu and Co edges mirrors those of Cu foil and Co_3O_4, respectively (Fig. 3c and d). This result reveals the complete reduction of Cu species to Cu^0. It appears that the presence of Co_3O_4 does not support the XPS results revealing the presence of Co^0 and CoO phases, possibly because XAS was not performed during *in situ* catalyst reduction. Therefore, due to the high/strong oxophilicity of Co[39,40], it easily underwent oxidation. Additionally, the observed shifts in the white line energy (8994.14 eV for Co_5CuAl *vs.* 8993.52 eV for Cu foil, and 7729.12 eV for Co_5CuAl *vs.* 7729.51 eV for Co_3O_4) suggest Co–Cu interaction and the formation of the CoCu alloy in the Co_5CuAl LDO catalyst.[41,42]

Based on the extended X-ray absorption fine structure (EXAFS) spectra and the fitted parameters (Fig. 3e and f, Fig. S5, and Tables S2 & S3†), the presence of the Co–Cu bond in the EXAFS spectra of the Co and Cu K-edges distinctly confirms the formation of the CoCu alloy in the Co_5CuAl catalyst. Interestingly, copper forms a fully alloyed species at 2.53 Å with a coordination number of 6.5, while cobalt shows alloying at 2.51 Å with a coordination number of 1, likely due to the lower concentration of Cu in the catalyst.

HMF hydrogenation/hydrogenolysis reactions

As seen in the catalyst screening tests (Fig. 4a), under the applied reaction conditions, both the monometallic CuAl and CoAl catalysts were mainly selective in producing BHMF (with yields of 89% and 66%, respectively), indicating hydrogenation of HMF's carbonyl group (Scheme 1; P-1). Compared with the CuAl catalyst, the CoAl catalyst was capable of hydrogenating the furan ring and facilitating ring-opening hydrogenolysis to some extent, resulting in ~13% and ~8% yields of BHMTHF and 1,2,6-HTO, respectively. This difference can be attributed to the variation in the hydrogen/HMF adsorption energy and configuration which will be discussed later. In contrast, for reactions using Co_xCuAl, increasing the amount of cobalt led to a gradual reduction of BHMF yield, accompanied by a continuous increase in the yield of 1,2,6-HTO, with Co_5CuAl achieving ~50% yield. These results imply the significance of Co–Cu interaction and the formed CoCu alloy in enhancing the H_2 adsorption/activation capability (Fig. 2b & 7a–d) and influencing the substrate adsorption capacity/mode on the bimetallic catalyst (to be discussed later). However, further increasing the Co/Cu ratio to 10 led to a ~5% decline in 1,2,6-HTO yield. From the results obtained with bimetallic LDO catalysts, the primary conclusion is that the formed CoCu alloy can catalyze both hydrogenation of the carbonyl group, producing BHMF as an intermediate (Scheme 1; P-1), and ring-opening hydrogenolysis of BHMF, producing 1,2,6-HTO (Scheme 1; P-4). In contrast, the monometallic CuAl and CoAl catalysts, which lack the CoCu alloy phase, are unable to facilitate the ring-opening reaction. Further investigations, detailed in the computational section, confirm that electron-enriched Co or electron-deficient Cu within the CoCu alloy constitutes the prominent active site. It is worth noting that in all catalyst screening tests, a minor pathway was observed in which the

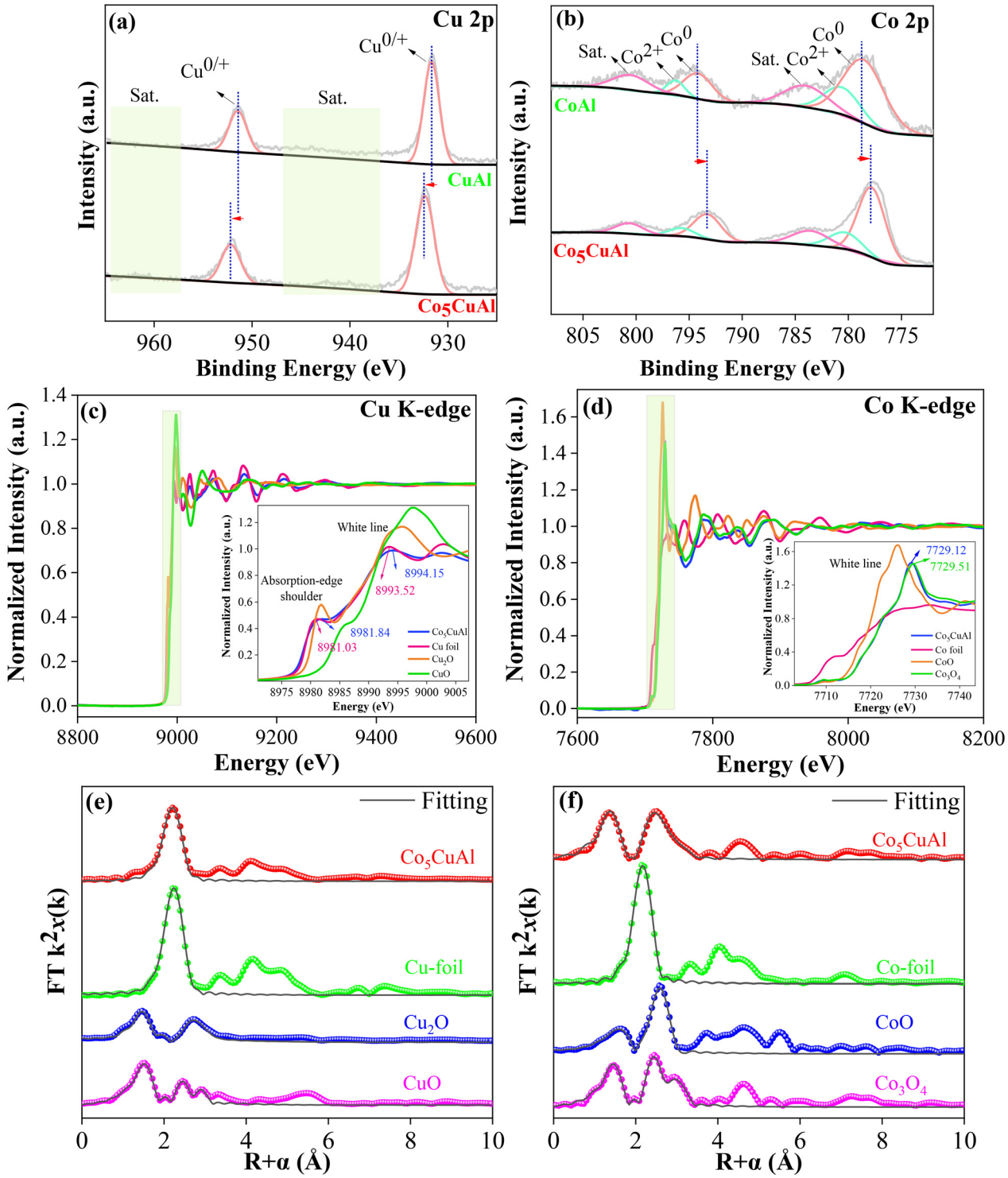

Fig. 3 *In situ* XPS spectra of (a) Cu 2p and (b) Co 2p for the CuAl, CoAl, and Co_5CuAl catalysts. Cu and Co K-edge XANES (c and d) and EXAFS spectra (e and f) of the Co_5CuAl catalyst and standard samples.

furan rings in BHMF underwent over-hydrogenation, potentially due to the parallel adsorption of BHMF on the catalyst to some extent,[12] resulting in the formation of BHMTHF (Scheme 1; P-2). To further investigate the synergetic effect of Co and Cu metals, a reaction using a physical mixture of monometallic CoAl and CuAl catalysts (Co/Cu molar ratio 5) was also performed, where the main product was BHMF, revealing the significance of the Co–Cu pair site of the CoCu alloy in the bimetallic LDO catalysts for facilitating the desirable ring-opening reaction.

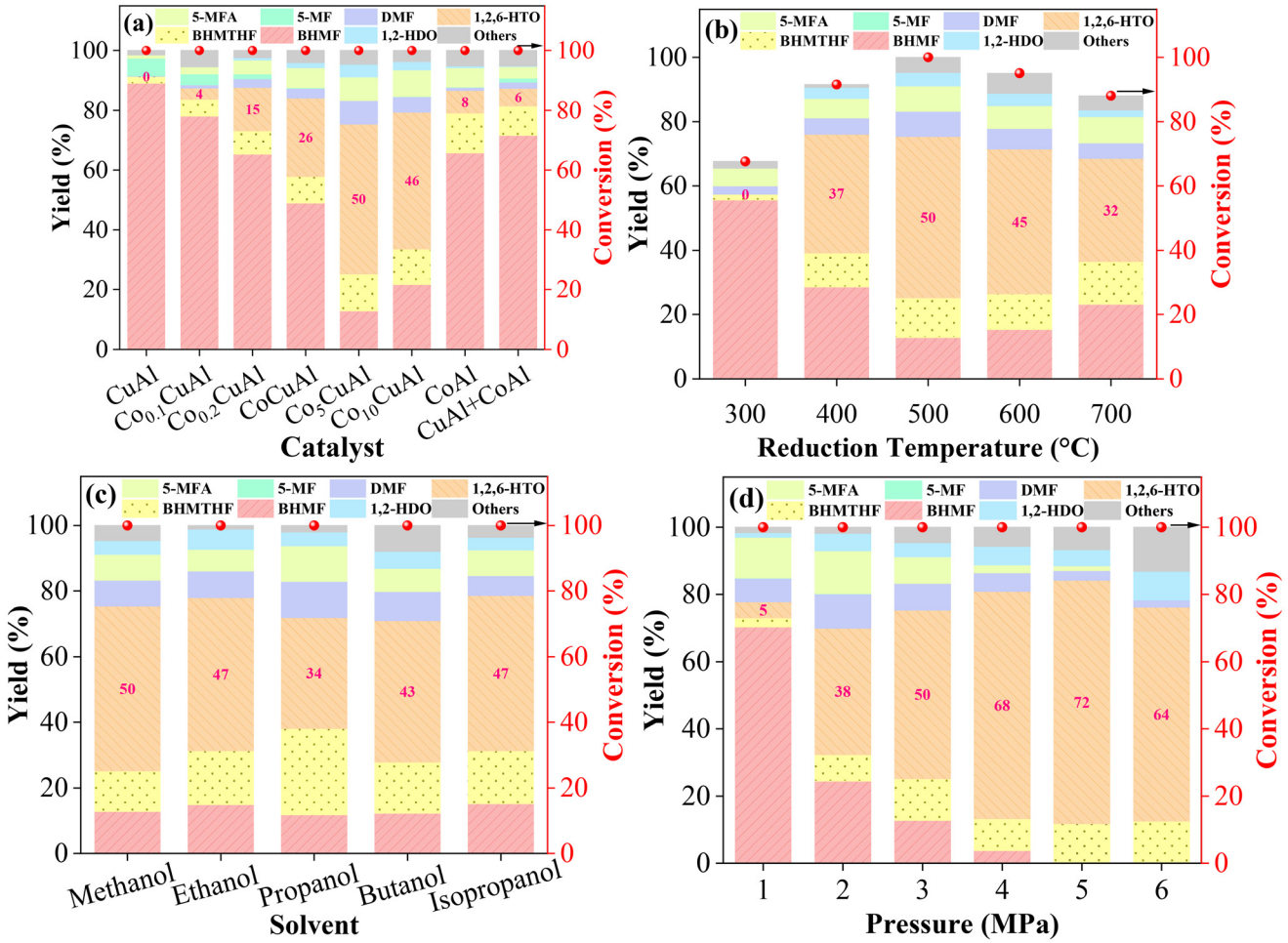

Fig. 4 Effects of the (a) LDO composite and (b) Co_5CuAl reduction temperature on HMF hydrogenation/hydrogenolysis. Reaction conditions: 30 mg catalyst, 10 mL methanol, 1 mmol HMF, 120 °C, 3 h, 3 MPa H_2. Effects of (c) solvent and (d) H_2 pressure on HMF hydrogenation/hydrogenolysis. Reaction conditions: 30 mg Co_5CuAl, 10 mL solvent, 1 mmol HMF, 120 °C, 3 h ((c) 3 MPa H_2, (d) methanol).

Acid sites are another factor reported to catalyze the furan ring-opening (C–O cleavage).[43] However, based on our investigations (NH_3-TPD; Fig. S6 & Table S4†), it can be observed that while the acidity of CoAl was the highest, it showed poor performance in the ring-opening process. Therefore, it may be concluded that the acid sites are not crucial in the proposed catalytic system, and the interaction of metal sites, along with the subsequently formed alloy, is the crucial parameter.

Herein, Co_5CuAl was selected as the best catalyst, and then the effect of the catalyst reduction temperature on its performance was investigated (Fig. 4b). As seen, at a low reduction temperature of 300 °C, the conversion of HMF was low, producing mainly BHMF, likely due to the incomplete reduction of Co_3O_4 and insufficient formation of Co–Cu interactions (alloy) as the active site for the hydrogenation/ring-opening hydrogenolysis reactions. The HMF conversion and 1,2,6-HTO yield were remarkably increased at a reduction temperature of 400 °C, reaching complete conversion and ~50% 1,2,6-HTO yield at 500 °C. However, further increasing the reduction temperature to 600 °C and 700 °C led to a decrease in catalytic activity, which could result from the agglomeration of the catalyst and increase in the size of the Co and Cu particles, affecting the catalyst performance.[44]

Next, the effect of organic solvents on the catalytic performance was explored (Fig. 4c). Interestingly, all the tested solvents, except propanol, were effective at achieving complete HMF conversion and ~43–50% yield of 1,2,6-HTO. Using propanol also resulted in a high yield of BHMTHF (~27%), revealing increased hydrogenation of the BHMF furan ring compared to other alcohols, which could be due to the variation in the electron release-induced effect and the hydrogen bond donor capacity of the tested solvents.[45] It is noteworthy that water was also tested, resulting in less than 50% HMF conversion, mainly producing 5-MFA and DMTHF as byproducts, similar to the findings of Guo *et al.*, who reported that water led to poor activity in HMF conversion/hydrogenolysis,[46] likely due to the lower solubility of HMF and hydrogen in water, as well as the instability or deactivation of the proposed catalysts in the aqueous system.[46,47] Therefore, methanol was chosen in this work for the rest of the experiments owing to its low price

and boiling point, which make it cost-effective and easy to reuse.

The effects of H_2 pressure on HMF hydrogenation/hydrogenolysis are depicted in Fig. 4d. As shown, even at low hydrogen pressure (1 MPa), HMF conversion was complete, revealing the dual function of methanol, serving as both a solvent and a hydrogen donor.[48,49] At low pressure, HMF was mainly converted into BHMF through hydrogenation of the carbonyl group, while at higher pressure, the enhanced ring-opening capability led to a notable ~72% yield of 1,2,6-HTO under 5 MPa H_2. However, a further increase in H_2 pressure led to a drop in 1,2,6-HTO yield (~64%) and carbon balance, likely due to side reactions, resulting in byproduct formation (*e.g.*, DMTHF and 1-hexanol). Notably, the H-donating ability of methanol was further confirmed by conducting the reaction under 3 MPa N_2, where despite the significant decrease in the conversion of HMF and the changes in the main product, the converted HMF transformed into 5-MFA (Fig. S7†), revealing that the hydrogenated product could result from the hydrogen-donating ability of the methanol solvent in the absence of H_2 gas. Indeed, it can be concluded that HMF is catalyzed *via* hydrogen from both H_2 gas and methanol, where the efficiency of the proposed system (conversion and product selectivity) is much more promising when H_2 gas is introduced in the system.

Fig. 5a depicts the effects of reaction time/temperature on the distribution of products obtained from HMF transformation over the Co_5CuAl catalyst. Under all the conditions tested, HMF was entirely converted, while the selectivity of the desired product was tunable *via* changing the reaction time/temperature. At 80 °C and 1 h, the main product was BHMF, with a yield of ~91%, indicating that carbonyl group hydrogenation was the main reaction under these conditions. However, extending the reaction time to 5 h at the mentioned temperature led to a reduced yield of BHMF due to over-hydrogenation and/or hydrogenolysis reactions, producing 1,2,6-HTO and BHMTHF with yields of ~50% and ~26%, respectively. At temperatures ≥100 °C and longer reaction times, however, the carbon balance gradually declined due to side reactions, and consequently, byproducts were formed. In particular, the reaction at 140 °C formed DMF with 8–16% yield due to hydrodeoxygenation of 5-MFA.[50] On extending the reaction time, the yield of 1,2,6-HTO consistently increased at lower temperatures (80 °C and 100 °C), while it reached a plateau and then declined within the 1–5 h range at elevated reaction temperatures (120 °C and 140 °C), due to hydrodeoxygenation of 1,2,6-HTO into diols (*e.g.*, 1,2-/1,5-/1,6-HDOs) and/or hexane. Therefore, using the Co_5CuAl catalyst, switchable production could be achieved by tuning the reaction temperature/time, resulting in ~91% and ~72% yields of BHMF (1 h, 80 °C) and 1,2,6-HTO (3 h, 120 °C), respectively (Fig. 5a and b). Thus, it can be inferred that the CoCu alloy within Co_5CuAl initially catalyzes the hydrogenation of HMF's carbonyl group to form BHMF as the main product (Scheme 1; P-1), while on extending the reaction time and/or increasing the temperature, BHMF undergoes conversion to 1,2,6-HTO through ring-opening hydrogenolysis catalyzed by this alloy (Scheme 1; P-4). Additionally, there could be another possible reaction route where BHMF is fully hydrogenated to BHMTHF (Scheme 1; P-2), and then BHMTHF is converted into 1,2,6-HDO through ring-opening (Scheme 1; P-3), which will be further studied later.

Upon comparing the activity of the synthesized Co_5CuAl catalyst with those reported in the literature (Table 1), we found that our new catalyst demonstrated promising performance in hydrogenation/hydrogenolysis of HMF into BHMF/1,2,6-HTO products with tunable selectivity under mild reaction conditions. To quantitatively assess the improved performance of the catalyst, a term *specific productivity* was introduced, defined as the moles of BHMF or 1,2,6-HTO formed per unit of reaction time and total catalyst mass. As shown in Table 1, the *specific productivity* of the Co_5CuAl catalyst for BHMF yield (30.4) is comparable to that reported in the literature, while the value for 1,2,6-HTO yield (8.0) is higher than that (~0.3–7.8) reported in the literature. Thus, our catalyst exhibited a unique ability to achieve selective production of

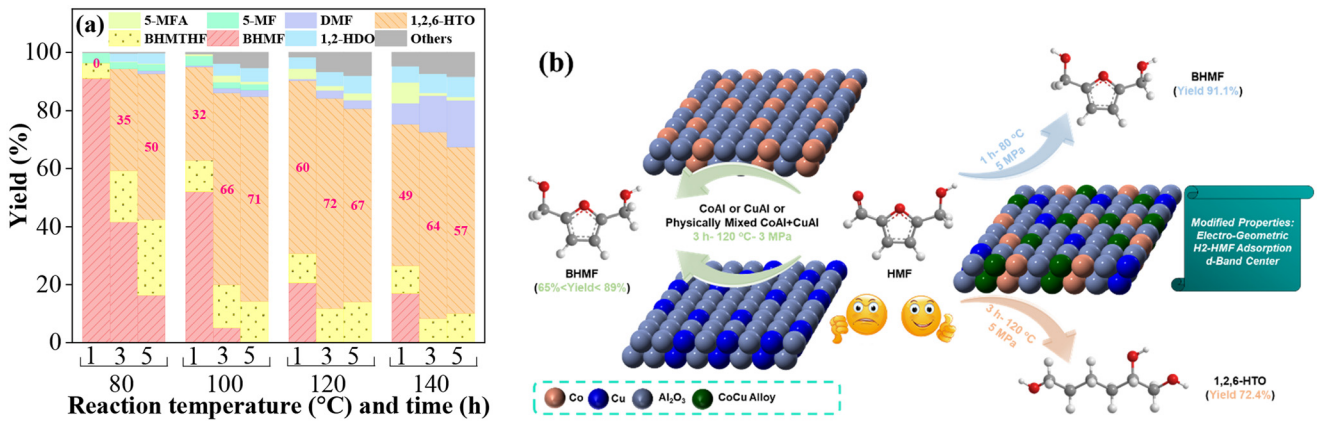

Fig. 5 (a) Effects of time/temperature on HMF hydrogenation/hydrogenolysis. Reaction conditions: 30 mg Co_5CuAl, 10 mL methanol, 1 mmol HMF, 5 MPa. (b) Schematic diagram of the catalytic hydrogenation/hydrogenolysis of HMF into BHMF and/or 1,2,6-HTO.

Table 1 Summary of the literature works on HMF hydrogenation/hydrogenolysis into BHMF/1,2,6-HTO using noble/non-noble metal catalysts

Catalyst	Reaction time (h)	Reaction temperature (°C)	Reaction pressure (MPa)	BHMF yield (%)	1,2,6-HTO yield (%)	Specific productivity[b] (mmol g^{-1} h^{-1})	Ref.
Ru/C	1	100	2	80.2	—	31.8	52
Ru/Co_3O_4	6	190	—[a]	82.8	—	2.2	8
Pt/CeO_2–ZrO_2	8	170	1	97	—	0.75	53
Cu/Al_2O_3	1	130	3	93	—	14.5	54
CuZn	3	120	7	95	—	12.5	55
ZrCa@CNS	10	190	—[a]	84.2	—	~0.1	56
NiGaAl	1	140	3	95.6	—	31.9	57
Co_5CuAl	**1**	**80**	**5**	**91.1**	**—**	**30.4**	**This work**
$Co–Pt/CeO_2$	24	135	3	—	42	~0.4	9
$Pt@Al_2O_3$	24	35	—	—	63	~0.3	58
$Ni-Ce/Al_2O_3$ + CaO	1	190	5	—	59	7.8	59
NiCoAl	12	120	4	—	64.5	2.1	12
Co5CuAl	3	120	5	—	72.4	8.0	This work

[a] Catalytic transfer hydrogenation (CTH) system. [b] Specific productivity = (BHMF or 1,2,6-HTO [mmol])/(time [h] × catalyst mass [g]).

the desired product through the precise adjustment of reaction conditions, without the need to alter the catalyst composition.

Encouraged by the results obtained, we also investigated the catalytic hydrogenation/hydrogenolysis of furfural (FF), another biomass-derived furanic platform chemical for which selective conversion poses a challenge.[51] Under the applied reaction conditions (3 h, 120 °C, 5 MPa) and using the Co_5CuAl catalyst, FF was fully converted, and furfuryl alcohol (FFA), tetrahydrofurfuryl alcohol (THFA), 1,5-pentanediol (1,5-PDO), and 1,2-pentanediol (1,2-PDO) were detected as the main products (Fig. S8†), revealing both the hydrogenation and ring-opening hydrogenolysis capabilities of the proposed catalyst for various bio-based furanic chemicals. It is worth mentioning that the investigation of the effect of reaction parameters (time, temperature, pressure, *etc.*) on the product distribution (open-ring and hydrogenated products) needs to be conducted systematically, as this is crucial for future research endeavors.

The Co_5CuAl catalyst's reusability was evaluated over four cycles with the specified reaction parameters. According to the VSM analysis (Fig. S9a†), in which the saturation magnetization (M_s) and coercivity (H_c) values are 14.23 emu g^{-1} and 50.33 Oe, respectively, as well as the inset picture, the catalyst exhibited significant magnetic properties that enable its easy recycling by magnetic separation, demonstrating promise for future large-scale applications. The results (Fig. S9b†) revealed that, although the HMF conversion remained complete throughout the four cycles, the yield of 1,2,6-HTO dropped substantially and reached ~29% after the fourth cycle, suggesting catalyst deactivation due to the deposition of polymeric substances and/or metal leaching. In the fifth run, the regenerated catalyst was tested, and it showed activity that was comparable to that in the initial cycle, which confirms the stability of the catalyst's structure and its resistance to severe metal leaching. This was further confirmed by comparing the XRD patterns (Fig. S9c†) and the ICP results (<3% total metal leached; Table S5†) of the fresh and regenerated catalysts. TGA analysis (Fig. S9d†) indicated the presence of carbonaceous materials on the spent catalyst's surface, thus leading to the blockage of CoCu alloy active sites, which could be the main cause of catalyst deactivation during cycling tests.

Structure–activity correlation

Adsorption tests were performed to examine the relationship between the catalysts and their capability for HMF adsorption, and the results are illustrated in Fig. 6a and b. The adsorption capacities of the CuAl, CoAl, and Co_5CuAl LDO catalysts for HMF were found to be 1.1, 1.7, and 2.6 mg g^{-1}, respectively. Accordingly, the adsorption quantity of HMF on the Co_5CuAl catalyst was significantly higher than those on the other two catalysts, implying that the formed CoCu alloy in the bimetallic catalyst can enhance not only H_2 activation (Fig. 2b & 7a–d) but also substrate adsorption, thereby accelerating HMF hydrogenation and subsequent ring-opening hydrogenolysis reactions. It should be noted that normalization of the HMF adsorption capacity based on the catalysts' textural properties, SSA and pore volume, was also carried out, revealing that Co_5CuAl still demonstrated the highest value. One reason for the increased HMF adsorption on Co_5CuAl is the modified d-band center of the surface element and a different adsorption configuration compared to monometallic catalysts,[31] which will be confirmed in the subsequent section *via* DFT calculations.

According to the *in situ* CO-FTIR measurements (Fig. 6c), for the CuAl catalyst, two weak bands at 2117 and 2170 cm^{-1} were detected, indicating linear CO adsorption to Cu^0 and Cu^+, respectively.[60] For the CoAl catalyst, a small peak at 1935 cm^{-1} and a broad peak at 2037 cm^{-1} were observed, representing bridge and linear CO adsorption to Co^0, respectively.[61] In contrast, the bimetallic Co_5CuAl catalyst showed no bridge band but displayed a noticeable blue-shift (for CO–Cu^0) and red-shift (for CO–Co^0), indicating electron transfer from Cu to Co, followed by Co–Cu interface (alloy) formation. The process of electron transfer alters the distribution of electrons in various atomic orbitals, subsequently modifying the d-band center of surface atoms.[62] This is followed by changes in the adsorption capacity for the reactant molecules, as shown in Fig. 6a and b, ultimately leading to varied catalytic performance (Fig. 4a).

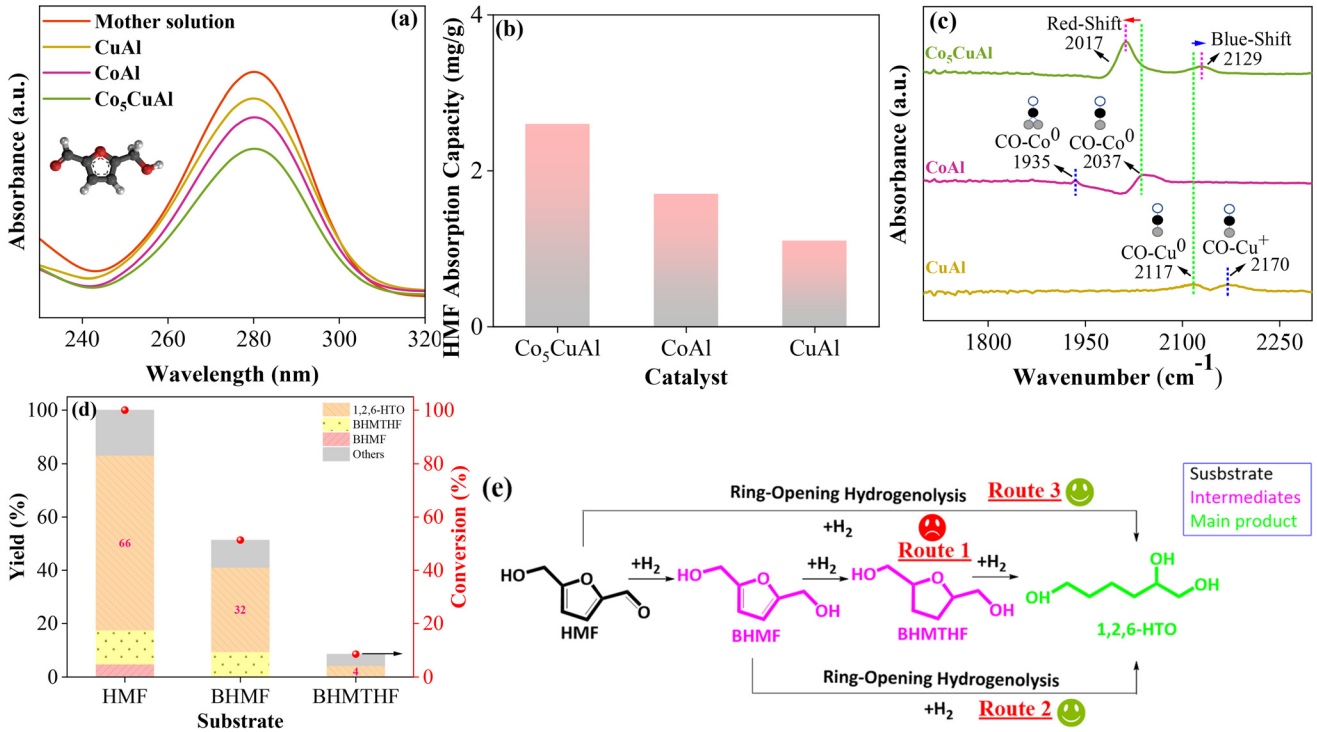

Fig. 6 (a) UV-vis spectra of the residual solutions after HMF adsorption, (b) HMF adsorption capacity, and (c) CO-FTIR after flushing with Ar for 5 min at 30 °C. (d) Hydrogenation/hydrogenolysis of HMF, BHMF, and BHMTHF over Co_5CuAl. Reaction conditions: 30 mg Co_5CuAl, 10 mL methanol,1 mmol substrate, 2 h, 120 °C, 5 MPa. (e) A plausible reaction pathway for HMF transformation into 1,2,6-HTO over Co_5CuAl.

In addition, controlled experiments were conducted to gain a better understanding of the reaction mechanism for the synthesis of 1,2,6-HTO, using HMF, BHMF, and BHMTHF as substrates under the same reaction conditions (Fig. 6d). As shown, while HMF was fully converted, the conversion of BHMTHF was less than 10%. This result implies that the conversion of HMF into 1,2,6-HTO *via* the HMF → BHMF → BHMTHF → 1,2,6-HTO pathway (Route 1) is very slow, as reported in other studies.[58,63] Using BHMF as a substrate however led to a relatively higher conversion (~50%), with the main detected products being 1,2,6-HTO (~32%) and BHMTHF (~10%) (Route 2), but the substrate conversion and 1,2,6-HTO yield were still much lower than those with the HMF substrate. These results thus suggest another new reaction route in this catalytic system where HMF can be converted through HMF ring-opening hydrogenolysis into 1,2,6-HTO (Route 3, without BHMF as an intermediate).

Accordingly, in our proposed catalytic system, we have elucidated the existence of three parallel reaction pathways (Fig. 6e). Notably, the production of the BHMTHF intermediate is deemed undesirable and should consequently be restricted, whereas the other two pathways contribute to the efficient production of 1,2,6-HTO from HMF.

Computational simulation of the catalysts

According to the experimental/characterization results discussed in the previous sections, active sites including metallic Co, metallic Cu, and the CoCu alloy were considered for the DFT calculations, although the influence of Al and other oxide species was not taken into account. Models were constructed for Co(111), Cu(111), and CoCu(111) surfaces (as shown in Fig. S10†) to assess the adsorption energy of H and HMF on the catalysts (CoAl, CuAl, and Co_5CuAl, respectively) and determine the surface d-band center. In the CoCu model, a molar ratio of Co/Cu = 5 was considered, as it was identified as the optimal catalyst in experimental tests.

The initial calculations aimed to determine the d-band center value of the surface atoms (Fig. S11†). For the sole Co and Cu surfaces, these values were found to be −1.41 eV and −2.24 eV, respectively. On the CoCu alloy surface, the d-band values for Co and Cu were recorded as −1.37 eV and −2.76 eV, respectively, indicating electron transfer from Cu to Co, consistent with the results obtained using the characterization techniques (XPS, XAS, and CO-FTIR). Next, the adsorption energy of H atoms on these surfaces was calculated, with a hollow-face-centered cubic (FCC) crystalline structure, being the most stable site, applied in the calculations (Fig. 7a–d). The H adsorption energy on Co and particularly Cu surfaces was lower compared with that on the CoCu surface, that is, the CoCu surface can adsorb more H, which is in accordance with the results obtained from H_2-TPD, where the Co_5CuAl catalyst exhibited a larger peak area than the other two monometallic catalysts. Interestingly, Co on the CoCu surface exhibited a higher H adsorption energy than Cu on the CoCu surface. These results, in combination with the experimental data obtained, suggest that cobalt, being electron-rich, serves as a

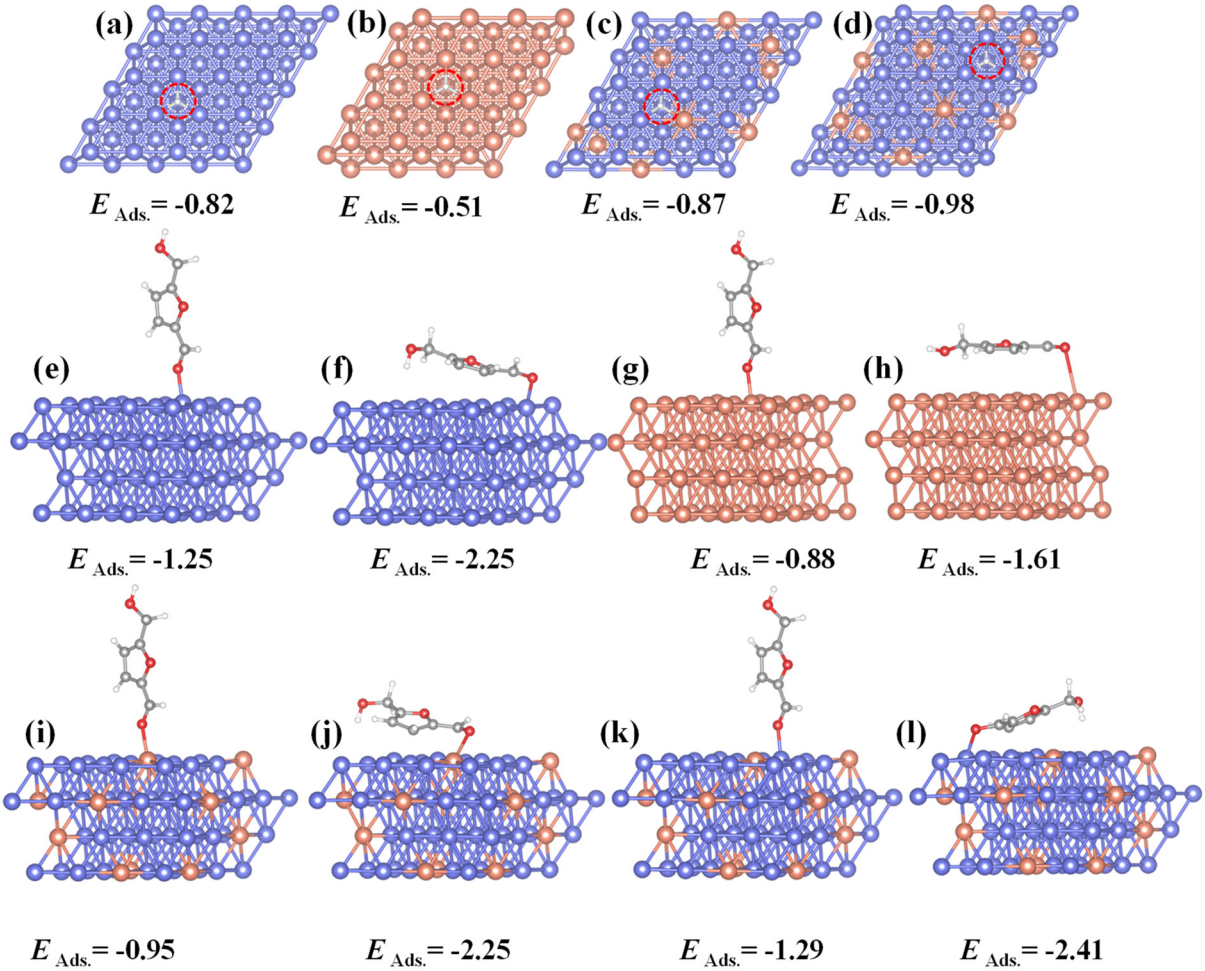

Fig. 7 Adsorption energies of H atoms on the surface of (a) Co(111), (b) Cu(111), (c) Cu of CoCu(111), and (d) Co of CoCu(111) (top view). Adsorption configurations/energies of HMF on the (e and f) Co(111), (g and h) Cu(111), (i and j) Cu of CoCu(111), and (k and l) Co of the CoCu(111) surface (side view).

more effective active site than copper (electron-deficient) for hydrogen activation and the subsequent HMF hydrogenation. It should be mentioned that on the CoCu(111) surface, it is not possible for H to be bonded only to Cu, so it has been bonded with both Cu and Co (Fig. 7c).

Subsequently, the adsorption configuration and energy of HMF on the surfaces were investigated. Based on the obtained experimental results, where CoAl and CuAl mainly produced BHMF, we explored a tilted/parallel configuration for the adsorption of HMF onto these surfaces, focusing on HMF's carbonyl group (adsorption through the furan ring was not considered). As observed (Fig. 7e–h), the adsorption energy of HMF on both Co(111) and Cu(111) *via* the parallel mode is not favorable, exhibiting the lowest adsorption energy. In contrast, adsorption in the tilted configuration is prominent, with the HMF adsorption energy on Co(111) being higher than that on Cu(111). This supports the obtained experimental results reported previously, where HMF adsorption on CoAl was higher than that on CuAl (Fig. 6a and b). These results also align with the measured d-band values, indicating that Co exhibited a higher d-band value than Cu (−1.41 eV *vs.* −2.24 eV; higher d-band value: minus sign with smaller number); hence, the CoAl catalyst can adsorb more HMF than the CuAl catalyst.

For the CoCu(111) surface, in addition to the adsorption configurations considered for Co(111) and Cu(111), the adsorption of HMF *via* its ring was also taken into account. This state was considered because of a reaction pathway involving HMF ring-opening, requiring some degree of HMF adsorption from its furan ring. Regarding the adsorption for the carbonyl group (Fig. 7i–l), similar to Co(111) and Cu(111), the adsorption energy on Co and Cu of the CoCu(111) surface *via* the parallel mode was the lowest. Stronger tilted adsorption was observed, with the adsorption energy of HMF on Cu and Co of CoCu(111) being −2.25 and −2.41 eV, respectively, demonstrating the higher capability of electron-rich Co for HMF adsorption than that of electron-deficient Cu in the Co_5CuAl catalyst. This can also be attributed to the higher d-band center value of Co than that of Cu on the CoCu(111) surface, as shown in Fig. S11.† The higher adsorption energy

on CoCu(111) than those on Co(111) and Cu(111) is in accordance with the adsorption tests and the better catalytic performance of Co_5CuAl over CoAl and CuAl, as confirmed in the experiments on hydrogenation/hydrogenolysis of HMF to 1,2,6-HTO. Admittedly, the HMF adsorption energy *via* its furan ring is low (Fig. S12†), suggesting that HMF adsorption through this mode is not favorable and this could not support one of the three reaction pathways (HMF ring-opening) proposed previously. This might however be due to influences of the reaction conditions (temperature and pressure), which were not taken into account in our theoretical calculations.

Overall, the obtained results from theoretical (DFT) calculations support experimental findings that the CoCu alloy formed within the CoCuAl catalyst can adsorb more HMF and activate more hydrogen than the monometallic CoAl and CuAl catalysts. This can be attributed to the electro-geometric changes in the catalysts, where the electron-enriched Co has a higher d-band value, enabling it to adsorb more substrates and accelerate the hydrogenation/ring-opening hydrogenolysis reactions.

Conclusions

In this work, Co_xCuAl LDO catalysts were introduced for the first time for hydrogenation and ring-opening hydrogenolysis of HMF to BHMF and 1,2,6-HTO in a one-pot process with tunable selectivity. While the monometallic CoAl and CuAl and physically mixed CoAl + CuAl catalysts predominantly favored BHMF production (65–89% yield) through hydrogenation of HMF's carbonyl group, the tailored Co_5CuAl catalyst achieved efficient and switchable production of BHMF (~91% at 1 h and 80 °C) and 1,2,6-HTO (~72% at 3 h and 120 °C) *via* tuning the reaction conditions, which can be attributed to a robust Co–Cu interaction accompanied by modified electro-geometric properties. Indeed, the electron-rich Co within the formed CoCu alloy was active for both efficient hydrogenation and ring-opening hydrogenolysis, while due to the lack of this active site in monometallic catalysts, only the hydrogenated product (BHMF) could be achieved. The catalyst demonstrated acceptable reusability and stability after regeneration. The adsorption experiments and DFT calculations revealed that the bimetallic catalyst exhibited a superior activity for HMF/H adsorption compared to the monometallic catalysts, owing to the formation of the CoCu alloy, which resulted in a higher d-band center attributed to the electron-enriched Co. Controlled tests demonstrated the existence of three parallel reaction pathways for HMF conversion into 1,2,6-HTO. Therefore, these findings and future advancement of this work would lead to the development of a novel one-pot process for efficient and switchable production of biochemicals from HMF.

Author contributions

Armin Rezayan: investigation, methodology, data curation, formal analysis, and writing – original draft. Zhen Zhang; Xiaomeng Yang: formal analysis and discussion. Dan Wu; Renfeng Nie; Tianliang Lu; Jianshe Wang; Xiaoqin Si: discussion and writing – review & editing. Yongsheng Zhang; Chunbao Xu: conceptualization, investigation, supervision, and project administration.

Data availability

All data are available in the manuscript and the ESI.†

Conflicts of interest

There are no conflicts to declare.

Acknowledgements

The authors acknowledge the financial support from the National Key R&D Program of China (No. 2022YFC2104505), the National Natural Science Foundation of China (No. 52074244), and the startup grant from the City University of Hong Kong (9380159).

References

1 Q. Hou, X. Qi, M. Zhen, H. Qian, Y. Nie, C. Bai, S. Zhang, X. Bai and M. Ju, *Green Chem.*, 2021, **23**, 119–231.
2 Y. Wang, H. Wang, X. Kong and Y. Zhu, *ChemSusChem*, 2022, **15**, e202200421.
3 W. Zhao, F. Wang, K. Zhao, X. Liu, X. Zhu, L. Yan, Y. Yin, Q. Xu and D. Yin, *Carbon Resour. Sci.*, 2023, **6**, 116–131.
4 T. Buntara, I. Melián-Cabrera, Q. Tan, J. L. G. Fierro, M. Neurock, J. G. de Vries and H. J. Heeres, *Catal. Today*, 2013, **210**, 106–116.
5 Y. Zheng, L. Wang, H. Liu, J. Yang, R. Zhang, L. Zhang and Z. A. Qiao, *Angew. Chem.*, 2022, **134**, e202209038.
6 B. Xiao, M. Zheng, X. Li, J. Pang, R. Sun, H. Wang, X. Pang, A. Wang, X. Wang and T. Zhang, *Green Chem.*, 2016, **18**, 2175–2184.
7 A. A. Turkin, E. V. Makshina and B. F. Sels, *ChemSusChem*, 2022, **15**, e202200412.
8 T. Wang, J. Zhang, W. Xie, Y. Tang, D. Guo and Y. Ni, *Catalysts*, 2017, **7**, 92.
9 H. Kataoka, D. Kosuge, K. Ogura, J. Ohyama and A. Satsuma, *Catal. Today*, 2020, **352**, 60–65.
10 A. M. Ruppert, K. Weinberg and R. Palkovits, *Angew. Chem., Int. Ed.*, 2012, **51**, 2564–2601.
11 Q. Wang, J. Feng, L. Zheng, B. Wang, R. Bi, Y. He, H. Liu and D. Li, *ACS Catal.*, 2020, **10**, 1353–1365.
12 S. Yao, X. Wang, Y. Jiang, F. Wu, X. Chen and X. Mu, *ACS Sustainable Chem. Eng.*, 2014, **2**, 173–180.
13 F. Cai and G. Xiao, *Catal. Sci. Technol.*, 2016, **6**, 5656–5667.
14 S. Srivastava, G. C. Jadeja and J. Parikh, *RSC Adv.*, 2016, **6**, 1649–1658.

15 G. Gao, J. Remón, Z. Jiang, L. Yao and C. Hu, *Appl. Catal., B*, 2022, **309**, 121260.
16 K. Y. Kim, W. Jang, W. J. Byun, J. Y. Lee, M. Kim, J. H. Lee, G. B. Rhim, M. H. Youn, D. H. Chun, S. K. Kim, S. Cho and J. S. Lee, *ACS Catal.*, 2024, **14**, 7020–7031.
17 L. Luo, Y. Wang, M. Zhu, X. Cheng, X. Zhang, X. Meng, X. Huang and H. Hao, *Ind. Eng. Chem. Res.*, 2019, **58**, 8699–8711.
18 B. Ravel and M. Newville, *J. Synchrotron Radiat.*, 2005, **12**, 537–541.
19 A. García-Zaragoza, C. Cerezo-Navarrete, P. Oña-Burgos and L. M. Martínez-Prieto, *Nanoscale*, 2023, **15**, 12319–12332.
20 G. Kresse and J. Furthmüller, *Comput. Mater. Sci.*, 1996, **6**, 15–50.
21 J. P. Perdew, K. Burke and M. Ernzerhof, *Phys. Rev. Lett.*, 1996, **77**, 3865.
22 P. E. Blöchl, *Phys. Rev. B:Condens. Matter Mater. Phys.*, 1994, **50**, 17953.
23 S. Grimme, J. Antony, S. Ehrlich and H. Krieg, *J. Chem. Phys.*, 2010, **132**, 154104.
24 K. Sun, X. Gao, Y. Bai, M. Tan, G. Yang and Y. Tan, *Catal. Sci. Technol.*, 2018, **8**, 3936–3947.
25 Y. Ma, L. Wang, J. Ma, H. Wang, C. Zhang, H. Deng and H. He, *ACS Catal.*, 2021, **11**, 6614–6625.
26 M. Kalong, P. Hongmanorom, S. Ratchahat, W. Koo-amornpattana, K. Faungnawakij, S. Assabumrungrat, A. Srifa and S. Kawi, *Fuel Process. Technol.*, 2021, **214**, 106721.
27 L. Zhao, J. Duan, Q. Zhang, Y. Li and K. Fang, *Ind. Eng. Chem. Res.*, 2018, **57**, 14957–14966.
28 Y. Wei, S. Li, J. Jing, M. Yang, C. Jiang and W. Chu, *Catal. Lett.*, 2019, **149**, 2671–2682.
29 J. Zhao, Y. Bai, Z. Li, J. Liu, W. Wang, P. Wang, B. Yang, R. Shi, G. I. Waterhouse and X. D. Wen, *Angew. Chem., Int. Ed.*, 2023, **62**, e202219299.
30 A. Bulut, M. Yurderi, İ. E. Ertas, M. Celebi, M. Kaya and M. Zahmakiran, *Appl. Catal., B*, 2016, **180**, 121–129.
31 C. Wang, L. Li, X. Yu, Z. Lu, X. Zhang, X. Wang, X. Yang and J. Zhao, *ACS Sustainable Chem. Eng.*, 2020, **8**, 8256–8266.
32 L. N. Stepanova, R. M. Mironenko, E. O. Kobzar, N. N. Leont'eva, T. I. Gulyaeva, A. V. Vasilevich, A. N. Serkova, A. N. Salanov and A. V. Lavrenov, *Eng*, 2022, **3**, 400–411.
33 S. Sankaranarayanan, A. Sharma and K. Srinivasan, *Catal. Sci. Technol.*, 2015, **5**, 1187–1197.
34 C. Göbel, S. Schmidt, C. Froese, Q. Fu, Y.-T. Chen, Q. Pan and M. Muhler, *J. Catal.*, 2020, **383**, 33–41.
35 J. Akil, C. Ciotonea, S. Siffert, S. Royer, L. Pirault-Roy, R. Cousin and C. Poupin, *Catal. Today*, 2022, **384**, 97–105.
36 S. Li, H. Wang, W. Li, X. Wu, W. Tang and Y. Chen, *Appl. Catal., B*, 2015, **166–167**, 260–269.
37 Z.-H. He, N. Li, K. Wang, W.-T. Wang and Z.-T. Liu, *Mol. Catal.*, 2019, **470**, 120–126.
38 P. Ling, Q. Zhang, T. Cao and F. Gao, *Angew. Chem.*, 2018, **130**, 6935–6940.
39 W. Tu, M. Ghoussoub, C. V. Singh and Y.-H. C. Chin, *J. Am. Chem. Soc.*, 2017, **139**, 6928–6945.
40 W. J. Teo, X. Yang, Y. Y. Poon and S. Ge, *Nat. Commun.*, 2020, **11**, 5193.
41 Y. Shi, B. Luo, R. Liu, R. Sang, D. Cui, H. Junge, Y. Du, T. Zhu, M. Beller and X. Li, *Angew. Chem.*, 2023, **135**, e202313099.
42 N. Hashimoto, K. Mori and H. Yamashita, *J. Phys. Chem. C*, 2023, **127**, 20786–20793.
43 J. Tuteja, H. Choudhary, S. Nishimura and K. Ebitani, *ChemSusChem*, 2014, **7**, 96–100.
44 D. Li, Z. Wang, S. Jin and M. Zhu, *Chem Bio Eng.*, 2024, **1**, 541–547.
45 Y. Chen, Y. Zhang, W. Lin, X. Cheng, J. Wang, X. Liu, C. C. Xu and R. Nie, *Fuel*, 2023, **345**, 128136.
46 W. Guo, H. Liu, S. Zhang, H. Han, H. Liu, T. Jiang, B. Han and T. Wu, *Green Chem.*, 2016, **18**, 6222–6228.
47 P. Mäki-Arvela, D. Ruiz and D. Y. Murzin, *ChemSusChem*, 2021, **14**, 150–168.
48 Y. He, L. Deng, Y. Lee, K. Li and J. M. Lee, *ChemSusChem*, 2022, **15**, e202200232.
49 T. Pasini, A. Lolli, S. Albonetti, F. Cavani and M. Mella, *J. Catal.*, 2014, **317**, 206–219.
50 S. Xiang, L. Dong, Z.-Q. Wang, X. Han, L. L. Daemen, J. Li, Y. Cheng, Y. Guo, X. Liu and Y. Hu, *Nat. Commun.*, 2022, **13**, 3657.
51 J.-Y. Yeh, B. M. Matsagar, S. S. Chen, H.-L. Sung, D. C. W. Tsang, Y.-P. Li and K. C. W. Wu, *J. Catal.*, 2020, **390**, 46–56.
52 S. Fulignati, C. Antonetti, T. Tabanelli, F. Cavani and A. M. Raspolli Galletti, *ChemSusChem*, 2022, **15**, e202200241.
53 K. V. Vikanova, M. S. Chernova, E. A. Redina, G. I. Kapustin, O. P. Tkachenko and L. M. Kustov, *J. Chem. Technol. Biotechnol.*, 2021, **96**, 2421–2425.
54 K. T. V. Rao, Y. Hu, Z. Yuan, Y. Zhang and C. C. Xu, *Appl. Catal., A*, 2021, **609**, 117892.
55 G. Bottari, A. J. Kumalaputri, K. K. Krawczyk, B. L. Feringa, H. J. Heeres and K. Barta, *ChemSusChem*, 2015, **8**, 1323–1327.
56 J. Zhang, Z. Qi, Y. Liu, J. Wei, X. Tang, L. He and L. Peng, *Energy Fuels*, 2020, **34**, 8432–8439.
57 Y. Zhang, A. Rezayan, K. Wang, J. Wang, C. C. Xu and R. Nie, *ACS Catal.*, 2023, **13**, 803–814.
58 B. M. Matsagar, H.-L. Sung, J.-Y. Yeh, C.-T. Chen and K. C. W. Wu, *Sustainable Energy Fuels*, 2021, **5**, 4087–4094.
59 B. Pomeroy, M. Grilc and B. Likozar, *Green Chem.*, 2021, **23**, 7996–8002.
60 L. Cai, Z. Hu, P. Branton and W. Li, *Chin. J. Catal.*, 2014, **35**, 159–167.
61 J. A. Singh, N. Yang, X. Liu, C. Tsai, K. H. Stone, B. Johnson, A. L. Koh and S. F. Bent, *J. Phys. Chem. C*, 2018, **122**, 2184–2194.
62 R. Shu, R. Li, Y. Liu, C. Wang, P.-F. Liu and Y. Chen, *Chem. Eng. Sci.*, 2020, **227**, 115920.
63 B. Pomeroy, M. Grilc, S. Gyergyek and B. Likozar, *Appl. Catal., B*, 2023, **334**, 122868.